An Emerging Tropical Cyclone-Deadly Heat Compound Hazard

Matthews, T.[1*], Wilby, R.L.[1], Murphy, C.[2]

1. Department of Geography and Environment, Loughborough University, Loughborough, Leicestershire, United Kingdom, LE11 3TU
2. Irish Climate Analysis and Research UnitS (ICARUS), Department of Geography, Maynooth University, Maynooth, Co. Kildare, Ireland

*****Corresponding author

Word count (not including references or opening paragraph): **2,000**

Climate change may bring new hazards through novel combinations of extreme weather (compound events)[1]. Here we evaluate the possibility of dangerous heat following major tropical cyclones (TCs) – a combination with serious potential consequences given that mega-blackouts may follow powerful TCs[2], and the heavy reliance on air conditioning[3]. We show that "TC-heat" events are *already possible* along densely populated coastlines globally but, so far, only an estimated 1,000 people have been impacted. However, this number could rise markedly, with over two million at risk under a storyline of the observed TCs recurring in a 2°C warmer world than preindustrial. Using analogues as focussing events we show, for example, that if the catastrophic 1991 Bangladesh Cyclone occurred with 2°C global warming, there would be >70% chance of subsequent dangerous heat. This research highlights a gap in adaptation planning and a need to prepare for an emerging TC-heat compound hazard.

Extreme heat is a major threat to public health and a risk that is projected to rise with global warming[4], even if temperatures are held below the Paris targets of 1.5 or 2°C[5]. With around 1.6 billion units in operation, air conditioning (AC) reduces vulnerability to extreme heat[3,6]. However, populations dependent on AC may become highly exposed in the event of power failure[7]. Significant electricity outages have already been caused by Tropical Cyclones (TCs), with the top three events (2013 Typhoon Haiyan, 2017 Hurricane Maria, and 2012 Typhoon Bopha) incurring between 3.2 to 6.1 billion customer-hours of lost supply over one or two months[8–11]. Significant heat-related mortality was not reported during these mega-blackouts, but given the rapid rise in dangerous humid heat projected at low-latitudes[4], we identify the growing threat of a catastrophic "TC-heat" compound hazard. In this storyline, a TC first cripples electrical infrastructure, then is followed by deadly heat as the population tries to recover. Here, we provide the first assessment of the present and evolving risk of the TC-heat hazard under climate change.

We searched observational records (1979-2017) for compound TC-heat events, defined here as a major TC (central pressure ≤ 945 hPa) followed within 30 days by a Heat Index (HI) exceeding 40.6°C at the site of landfall (see Methods). We use the HI because of its widespread operational use, not least by the United States National Weather Service to communicate danger when values exceed 40.6°C. We employ the same threshold to define onset of potentially deadly conditions. According to our criteria, TC-heat events have been vanishingly rare, with only four of the 121 major TCs that made landfall followed by maximum HI ≥40.6°C (hereafter "HI40.6"). All these events were in remote northwest Australia (Fig. 1a), where around 1,000 people were exposed. Given that nearly 40 million people live in the paths of the 121 major TCs, and that almost 6 million of them are routinely exposed to HI40.6 (99.9th percentile of the HI ≥ 40.6°C; Fig. 1b), it is fortunate that so few have been exposed to a compound TC-heat event.

We investigated reasons for the infrequent overlap of TCs and HI40.6 using the North West Pacific (WP), South Indian (SI), and North Atlantic (NA) basins, which account for more than 85% of the TCs in our sample. Seasonal cycles of maximum TC probability and maximum HI40.6 occurrence are not generally in phase. In all three ocean basins, the maximum HI40.6 extent occurs before peak TC probability (Fig. 2). This is due to the different thermal inertias of land and ocean. Land heats up rapidly with the seasonal solar cycle; sea surface temperatures take longer to peak and remain elevated whilst the land and atmosphere begin to cool, creating an environment with increased convective available potential energy suitable for intense tropical cyclones[12,13]. Fig. 2 also reveals that the greatest overlap in seasonal curves of HI40.6 extent and major TC landfall probability is in the SI basin, suggesting that conditions there most favour TC-heat. This fits with our observation that northwest Australia (SI) is the only region to have experienced the hazard during the period of observations (Fig. 1a).

The rarity of TC-heat is due to asynchronous seasonal cycles of TC probability and HI40.6. Contrary to expectations[14], TCs do *not* reduce the probability of HI40.6 post landfall by modifying the thermodynamic environment (Fig. 3). TCs arrive after anomalously high HI from amplified air temperature and specific humidity. The average HI anomaly in the 30 days before landfall (0.45°C) is significantly different from zero according to a one-sample, two-tailed Student's *t*-test ($|t| = 4.52$, $p < 0.05$). TC passage then causes all variables except specific humidity to decrease, partially compensating the fall in air temperature, thereby maintaining the HI. After TC passage HI anomalies return to zero within approximately 10 days, and the mean anomaly in the 30-days after landfall (0.16°C) is *not* significantly different from zero ($|t| = 1.34$, $p = 0.18$). This *return* to the climatology results in a significant difference between HI anomalies before and after landfall according to a paired two-sample *t*-test ($|t| = 2.51$, $p < 0.05$). TC passage therefore reduces the HI, but only from unusually high values to conditions consistent with long-term averages. This implies that the probability of HI40.6 in the 30-days following TC landfall is *not* lower than the same 30-day window in other years. The finding is robust when re-analysed with data from nearby weather stations (see Supplementary Information).

A stochastic simulation was applied to gain deeper insight into the contemporary compound TC-heat hazard, and under climate change scenarios generated by pattern-scaling air temperature whilst holding relative humidity constant (e.g. ref. 15). Note that the *independence* between TCs and subsequent HI conditions means the *probability* of HI40.6

for each TC reduces to the climatological relative frequency of HI40.6 within 30 days of the landfall date. These probabilities can be summed over TCs to compute the *expected number* of TC-heat events for each 30-year period then used as weights to evaluate the expected number of people at risk (see Methods for details).

We find a rapid, non-linear increase in the number of TC-heat events as the climate warms (Fig. 4a). Under baseline conditions, the expected frequency is 0.10 compound events per year (3 events per 30-year climate normal period), which matches the observed rate. If the global mean temperature rises by 1.5 or 2°C above preindustrial, the expected frequency per 30-years becomes 7 and 11 events respectively. If global warming reaches 4°C (representing a high-emissions end-of-century scenario), TC-heat events could occur at least annually (Fig. 4a).

The rising frequency of TC-heat increases the number of people potentially affected (Fig. 4b). Under the 1.5 or 2°C global warming scenarios there could be respectively 1.2 or 2 million people at risk per 30-year period, rising to 11.8 million for 4°C. Using the baseline temperature anomaly (1981-2010: 0.68°C above preindustrial; see Methods) our analysis yields an expectation of 0.4 million people affected during 1979-2017, indicating that TC-heat is *already* possible along densely populated coastlines, and highlighting the good fortune that only approximately 1,000 people were affected over this period. We also anticipate an increase in the *intensity* of humid heat for people recovering from TCs. Fig. 4c shows that extreme HI values averaged across TC landfall sites post landfall (see Methods) could rise almost 2.5 times faster than global mean air temperature. As shown before, this is a consequence of the combined effect of rising air temperature and water vapour on humid heat[17,18].

Observed TC tracks (analogues) help demonstrate the evolving TC-heat hazard. We identified TCs that could *possibly* (*probability* > 0) or *probably* (*probability* > 0.5) be followed by HI40.6 under the different scenarios of warming (Fig. 5 and see Methods). *Possible* TCs under baseline conditions include very notable events, such as the 1991 Cyclone "Marian", which killed more than 138,000 people, affected over 15 million, and left around one million homeless[16]. Whilst the actual HI peaked at 37.9°C nine days after the TC made landfall in Bangladesh, the same 30-day window experienced HI40.6 in six separate years during 1981-2010. Neither the NA or WP basin have experienced a TC-heat event, but our results suggest there have been near misses, with Hurricane Emily (maximum HI = 38.3°C, 21 days after landfall) and Typhoon Rammasun (maximum HI = 39.9°C, six days after landfall) amongst those identified as *possible* analogues. Emily struck the Caribbean and Mexico in July 2005, impacting thousands and causing $billions of damage, including to electricity infrastructure[17]. After Rammasun made landfall in the Philippines (July, 2014), blackouts affected Manilla and complaints about the hot weather were reported in the media[18]. As expected from Fig. 2, early-season landfall is a common feature of these analogues. All but one of the 13 *possible* TCs in the WP, SI and NA occurred before the peak likelihood of a major TC landfall in each basin.

When the HI is scaled for global warming, many *possible* analogues transition to *probable*. Typhoon Rammasun and Hurricane Emily achieve this status with 1.5°C warming (*probable* at 1.25 and 1.5°C, respectively), whereas Cyclone Marian transitions under the 2°C scenario (at 1.75°C). Under a 4°C scenario, the number of *probable* analogues increases substantially. These include: 2017 Hurricane Harvey (at 2.25°C of warming) and 2005 Hurricane Katrina (at 3.5°C). At 4°C Typhoon Haiyan – cause of the largest blackout in history – becomes a *probable* analogue, with more than 70% likelihood of being followed by HI40.6.

Our assessment shows that TC-heat events are rare but already possible along some of the most densely-populated coastlines on Earth. For no change in TCs, the likelihood of TC-heat is expected to increase rapidly with warming, consistent with more frequent dangerous heatwaves in lower latitudes under climate change[4,15]. The growing dependence on AC in countries at risk of TCs[6] is therefore of concern, particularly so given that AC may decrease humans' natural thermal adaptability[7].

The threat of TC-heat may not be restricted to people affected by loss of AC. Some of the TCs mentioned displaced millions of people, and relief housing may not provide safe refuge from extreme heat[19]. Furthermore, humanitarian operations in the wake of TCs can involve large numbers of non-native personnel, such as the 7,600+ US troops arriving after Cyclone Marian[20]. People require several days to acclimatize and improve physiological response to extreme heat[21], placing such rescue workers at higher risk. Evacuations ahead of major TCs may also become progressively more dangerous with climate warming because our results show that the HI is anomalously high *before* major TCs make landfall.

Our assessment of evolving TC-heat is subject to some important caveats. First, we use the storyline of "no change" in TCs, yet *major* TCs are likely to become more frequent with warming[22]. Changes in seasonality are more uncertain[23], but the likelihood of TC-heat would be expected to increase more rapidly if future TCs occur earlier in the year (cf. Fig. 2). Second, our pattern-scaling assumes uniform changes across the temperature distribution and constant relative humidity. The even temperature increase is likely conservative because greater warming is expected at higher quantiles[24]. Climate model projections suggest modest reductions in mean relative humidity over land and even more subtle increases over ocean[25], supporting our constant relative humidity treatment, given the transitionary nature (ocean/land) of the coastal locations impacted by TCs. Even so, such statements refer to *mean* quantities, and little is known about relative humidity changes during extreme heat events in the low latitudes. Third, we assume a 2015 population, so our assessment reflects only the increasing hazard frequency and not the changing population exposure or their vulnerability. Low-latitude regions are projected to have rapid population growth over the 21st century, adding many more people to the regions with largest increases in deadly humid heat[26].

Overall, our assessment therefore provides a lower-bound estimate of the increasing number of people likely to be exposed to TC-heat as the climate warms. Understanding could be improved by assessing TC climatologies projected by next-generation ensembles of high-resolution, coupled physical models[27] or through downscaling[28]. TCs and humid heat are physically connected through moist enthalpy in the lower atmosphere[26,29], so future work focussing on this diagnostic under climate change could improve understanding of evolving risks in low latitudes. Future studies could also add more depth to the understanding of TC-heat impacts by explicitly modelling excess mortality as a function of humid heat, including the impact of increased vulnerability stemming from assumed AC loss[30].

Finally, our results present a simple but stark warning: with *no change* in TCs, but plausible rises in the HI, potentially deadly heatwaves are more likely to follow TCs and eventually strike vulnerable populations. Although a TC-heat event has not yet impacted a heavily-populated coastline the likelihood is growing. The absence of experience in dealing with such a compound hazard places those exposed communities at even greater risk[1]. By drawing attention to this emergent hazard, we trust that our study will stimulate further research and adaptation planning to protect those at growing risk from a TC-heat compound event.

Methods

Heat Index

Following previous climate change studies[15,31–33], we used the Heat Index (HI) to characterise humid heat under climate change. We calculated the HI as in ref. 34 by using 2m air temperature, 2m specific humidity, and surface pressure from the WFDEI dataset[35], which constitutes ERA-Interim reanalysis data[36] interpolated and corrected to land observations on a 0.5° × 0.5° grid. Specific humidity was converted into relative humidity using surface air pressure and the table look-up procedure ("RELHUM") available in the NCL programming language (version 6.5.0). WFDEI data are available for the period 1979-2015, so we extended the record to the end of 2017 by bias-correcting the ERA-Interim reanalysis[36], using the quantile mapping procedure described in ref. 37, but with separate correction functions derived for each calendar month. All corrections were applied at one percentile intervals.

Tropical Cyclones and Observations

The coordinates, distances to land, ocean basins, and central air pressures of TCs were extracted from IBTrACS Version 4 (beta), using data from 1979-2017 to overlap with the (extended) WFDEI record. Central air pressure was used to identify "major" landfalling TCs, defined as those whose centre was at some point over land whilst the pressure was no higher than 945 hPa (corresponding to at least a Category 3 Hurricane according to the Saffir Simpson Damage Potential Index[38]). We chose a definition of intensity based on central pressure because this variable is more consistently reported by different agencies than maximum sustained wind speeds[39]. This filtering procedure left us with 121 TCs.

The evolution of the surface meteorology at the sites of TC landfall was assessed by extracting time series from the nearest-neighbour land grid points in the WFDEI dataset for all time steps when the respective TC was over land and still of "major" status (i.e. ≤ 945 hPa). This process yielded 181 locations (grid points) across the 121 TCs. The number of land grid points impacted by each TC varied between one and six, although most (~91%) TCs impacted no more than two land grid points. The frequency of TC-heat events was then determined by the number of TCs that had HI>40.6°C in at least one grid cell during the 30 days after landfall. Note that 30 days is a conservative search window given that longer mega-blackouts have followed some TCs (see main text).

The number of people exposed to different HI values was assessed using the 0.042° × 0.042° (2.5 min) gridded 2015 population dataset available from ref. 40. For each of the 181 locations impacted by major TCs person-counts were extracted from all the 0.042° grid cells falling within the respective 0.5 × 0.5° WFDEI grid cell. In Figure 1b we show the number of people as a function of: (i) the maximum HI endured in the 30-days post TC landfall; and (ii) the all-time 99.9th percentile in the HI (a value occurring on average three days per decade). This general function can be written as:

$$Pop(HI) = \sum Pop_{i,j} \times f(\acute{HI}_{i,j} - HI) \qquad 1.$$

where Pop denotes the total population exposed to a heat hazard ($\acute{HI}$: either the maximum in the 30-days post TC landfall, or the all-time 99.9th percentile) of at least HI degrees Celsius; i and j are the 181 row/column indices of the population (and WFDEI) grid; and the function f evaluates to one when $\acute{HI}_{i,j}$ is less than HI, otherwise zero

To explore the rarity of compound TC-heat hazards, we computed day-of-year probabilities of major TC landfall for the North West Pacific, South Indian, and North Atlantic basins. These three oceans accounted for more than 85% of all major TC landfall events during the period 1979-2017. Probabilities were derived for each basin by counting for each day of the year (1-366) the number of times a TC made landfall somewhere in the basin then dividing the total by the number of years of TC data (n_{TC} = 2017−1979 + 1 = 39 years). We used the same approach to compute the mean day-of-year fraction of grid points experiencing HI40.6 in each basin. Note that only HI data from grid cells impacted by major TCs were considered in this averaging (see Fig. 2). These day-of-year series (probability of TC landfall, and fraction of grid points with HI40.6) were smoothed with a Gaussian kernel with standard deviation (σ) of 15/1.96 = 7.7 days, meaning that 95% of the kernel weight was applied to a one-month period centred on the day of interest. Smoothed series were then normalized by their respective maxima (Fig. 3).

The extent to which TC passage impacts the meteorological environment (Fig. 3) was assessed by screening anomalies at the 181 grid cells found to have experienced a major TC landfall during 1979-2017. We calculated anomalies by subtracting the seasonal cycle, generated by computing a day-of-year mean for each meteorological variable (1979-2017), before smoothing with the same Gaussian kernel (σ = 7.7 days).

The impact of each of the 121 TCs on the HI before and after landfall was evaluated statistically by averaging HI anomalies for the 30 days either side of their landfall date. We then subjected these before/after series, each comprised of 121 values, to a one sample *t*-test to investigate the null hypothesis that TCs do *not* cause the HI to be different from the climatology (i.e. that the population means for the anomalies were zero). The test statistic, t, was given by:

$$t = \frac{\overline{HI}}{\acute{\sigma}} \qquad 2.$$

where $\overline{HI}$ denotes the sample mean and $\acute{\sigma}$ is the sample standard deviation.

To investigate the *change* in HI following TC passage we also applied a dependent *t*-test for paired samples, for which *t* was computed:

$$t = \frac{\overline{\Delta HI}}{\Delta\acute{\sigma}} \qquad 3.$$

Where $\overline{\Delta HI}$ denotes the mean of the 121 paired differences between the before/after series, and $\Delta\acute{\sigma}$ is the standard deviation of these differences. In this instance, the null hypothesis was for no *change* in HI following TC passage (i.e. that the population mean of the paired differences in mean HI anomalies was zero). We used the Student's *t* distribution with 120 degrees of freedom to test these null hypotheses, concluding that TC impacts on the HI were statistically significant when $p \leq 0.05$.

Scaling the Heat Index to Simulate Climate Warming

We used pattern-scaling to explore the effect of climate warming on the probability of a compound TC-heat hazard. Temperatures, *T*, from the baseline climate (1981-2010) were re-scaled following:

$$T_{i,j,d,w} = T_{i,j,d} + \beta_{i,j,d}(w - c) \quad (4.)$$

Where i and j retain their meaning as WFDEI row/column indices, and d subscripts the day-of-year. The regression slope β quantifies the local change in running 30-year mean air temperature per degree of running 30-year average of the global mean air temperature. β was obtained at daily resolution by performing separate regressions for each month of the year, followed by linear interpolation of the slope coefficient to daily resolution. The regression analysis was performed with a sample of 58 CMIP5 model runs (see Supplementary Information for an inventory). We mainly used the ensemble mean in the analysis, but the 5th and 95th percentiles of β across the ensemble were also used to derive the uncertainty range in Fig. 4. The amount of climate warming (w) was incremented between 1 and 4°C in steps of 0.25°C. The constant subtracted from w (c = 0.68°C) represents the amount that 1981-2010 was warmer than pre-industrial (defined here as the average warming since 1880-1909 across the HadCRUT4[41], GISS[42] and BEST[43] datasets). Scaled T values from Equation (4) were used in the HI algorithm along with the original relative humidity to compute daily HI values under the warmer climates. Transforming the observed HI distribution in this way is consistent with previous studies[15,44], and has been shown to yield similar results at the global scale to daily-resolution projections of HI from climate models[15]. We prefer this scaling of observed HI over direct use of climate model integrations because of the considerable cold bias in modelled heat-humidity indices in the low-latitude domain of TCs[33].

Expected Frequency of Compound Hazard and Estimates of the Population at Risk

Observed independence between TC occurrence and subsequent HI conditions was represented within a stochastic simulation to gain deeper insight into the compound TC-deadly heat hazard for the present climate (baseline: 1981-2010) and under scenarios of global warming. We adopt this stochastic, observation-driven approach because observed TC tracks are not reproduced well by climate model simulations in the most complete global ensemble available (CMIP5)[22]. Moreover, even very high-resolution model simulations presently struggle to capture the important intricacies of the TC climatology required for assessment of the TC-heat hazard (such as TC seasonality in all basins or extent of sea-surface cooling)[45].

We computed the expected number of TC-heat events given the 121 TCs and the HI climatology using:

$$E[N] = \sum_{k=1}^{k=121} E[N_k] \quad (5.)$$

Where $E[N_k]$ is the expectation for each TC, defined (e.g. ref 46):

$$E[N_k] = \sum_{x} x\, p\{N_k = x\} \quad (6.)$$

in which p denotes probability, and *x* is either assigned the value of one (HI40.6 follows TC within 30 days), or zero (it does not). Setting $p_k = p\{N_k = 1\}$, it is clear that $E[N_k]$ is simply the probability of HI40.6:

$$E[N_k] = p_k \quad (7.)$$

We computed this probability using the observed climatology, extracting 1981-2010 WFDEI HI data from the sites of TC landfall for the 30-days following landfall date, irrespective of the year in which the TC occurred. This provides a 900-day ensemble of HI data (30 years of 30 days) for each of the 121 TCs. We then calculated how many times HI40.6 occurred at least once in each of the 30 years, yielding the probability of HI40.6:

$$p_k = \frac{1}{30} \sum_{y=1981}^{y=2010} \min\{1, \sum_{l=1}^{l=nloc} f(\mathrm{TC}_{k,l}, \mathrm{HI}_{k,l,y})\} \tag{8.}$$

where $nloc$ is the number of grid points impacted by the respective TC (indexed by *k*) and the function, *f*, evaluates to one if the maximum HI in the 30-day post-landfall sample in year *y* at landfall location *l* exceeds HI40.6, otherwise zero. Note that *nloc* ranges between one and six across all TCs.

To compute the expected number of people impacted by TC-heat ($E[P]$) we used:

$$E[P] = \sum_{k=1}^{k=121} E[P_k] \tag{9.}$$

where, P_k is the expected number of people for each TC, which is defined:

$$E[P_k] = \sum_{l=1}^{l=nloc} pop_{k,l} \;\; p_{k,l} \tag{10.}$$

in which $pop_{k,l}$ is the population estimate for grid point *l* impacted by TC *k*. Note that $p_{k,l}$ has the same meaning as in Eq. 7, although this time the *l* index highlights that probabilities are computed for *each location* impacted by the TC:

$$p_{k,l} = \frac{1}{30} \sum_{y=1981}^{y=2010} f(TC_{k,l}, \mathrm{HI}_{k,l,y}) \tag{11.}$$

$E[N]$ and $E[P]$ as calculated through equations 5 and 9 yield the expected number of TC-heat events and people impacted given the 121 major TC tracks and the climate of 1981-2010;

conversion to expected annual statistics was achieved by dividing by the number of years of TC data (1979 to 2017 = 39 years).

Whilst the HI40.6 metric enables us to track the changing *frequency* of compound TC-heat hazards, we recognise that populations may be differentially impacted by such events due to local variations in levels of acclimatization. Therefore, we also computed the changing *intensity* of humid heat, defined as the mean maximum HI in the 30-days following landfall, averaged across all 30-years and 121 TCs:

$$\overline{HI_{max}} = \frac{1}{30 \times 121} \sum_{k=1}^{k=121} \sum_{y=1981}^{y=2010} max(\mathrm{HI}_{k,y}) \quad 12.$$

We evaluated equations 5-12 using the baseline climate, before repeating them using the pattern-scaled climates to assess the changing TC-heat compound hazard as a function of global warming.

Analogues

We used analogues to explore regions at risk and the potential impact of the TC-deadly heat hazard. Analogues draw on known cases (the actual occurrence of the TC– complete with experienced impacts) to infer new consequences (the potential impacts of a TC followed by deadly heat). This approach can help non-specialists comprehend the unknown[15,47,48]. Here, we assigned the terms *possible* and *probable* to those TCs with $p_k > 0$ and $p_k > 0.5$, respectively. These analogues then illustrate potential impacts to raise awareness of the emerging TC-heat compound hazard.

Data Availability

The data that support the findings of this study are available from the corresponding author upon request.

References

1. Zscheischler, J. *et al.* Future climate risk from compound events. *Nature Climate Change* **8**, 469–477 (2018).
2. Houser, T. & Marsters, P. The World's Second Largest Blackout. *Rhodium Group* (2018). Available at: https://rhg.com/research/puerto-rico-hurricane-maria-worlds-second-largest-blackout/. (Accessed: 8th September 2018)
3. Barreca, A., Clay, K., Deschenes, O., Greenstone, M. & Shapiro, J. S. Adapting to climate change: the remarkable decline in the U.S. temperature-mortality relationship over the twentieth century. *Journal of Political Economy* **124**, 105–159 (2016).
4. Mora, C. *et al.* Global risk of deadly heat. *Nature Clim. Change* **7**, 501–506 (2017).
5. Vicedo-Cabrera, A. M. *et al.* Temperature-related mortality impacts under and beyond Paris Agreement climate change scenarios. *Climatic Change* **150**, 391–402 (2018).
6. International Energy Agency. *The Future of Cooling: Opportunities for energy-efficient air conditioning*. (2018).
7. Yu, J. *et al.* A comparison of the thermal adaptability of people accustomed to air-conditioned environments and naturally ventilated environments. *Indoor Air* **22**, 110–118 (2012).
8. Abi-Samra, N., McConnach, J., Mukhopadhyay, S. & Wojszczyk, B. When the bough breaks: managing extreme weather events affecting electrical power grids. *IEEE Power and Energy Magazine* **12**, 61–65 (2014).
9. The World's Second Largest Blackout. *Rhodium Group* (2018). Available at: https://rhg.com/research/puerto-rico-hurricane-maria-worlds-second-largest-blackout/. (Accessed: 1st July 2018)

10. US Department of Energy. *Hurricanes Maria and Irma November 20 Event Summary (Report #78)*. 1–5 (US Department of Energy, Infrastructure Secturity & Energy Restoration, 2017).
11. *Philippines: Typhoon Bopha*. (OCHA, 2013).
12. Emanuel, K. A. The maximum intensity of hurricanes. *J. Atmos. Sci.* **45**, 1143–1155 (1988).
13. Hart, R. E., Maue, R. N. & Watson, M. C. Estimating local memory of tropical cyclones through MPI anomaly evolution. *Mon. Wea. Rev.* **135**, 3990–4005 (2007).
14. Sriver, R. L. & Huber, M. Observational evidence for an ocean heat pump induced by tropical cyclones. *Nature* **447**, 577–580 (2007).
15. Matthews, T. K. R., Wilby, R. L. & Murphy, C. Communicating the deadly consequences of global warming for human heat stress. *PNAS* **114**, 3861–3866 (2017).
16. Guha-Sapir, D., Below, R. & Hoyois, P. EM-DAT: The CRED/OFDA International Disaster Database. (2018). Available at: www.emdat.be. (Accessed: 9th August 2018)
17. Beven, J. L. *et al.* Atlantic Hurricane Season of 2005. *Mon. Wea. Rev.* **136**, 1109–1173 (2008).
18. Morella, C. Power outages continue in Philippines following typhoon. *UCA News* (2014). Available at: https://www.ucanews.com/news/power-outages-continue-in-philippines-following-typhoon/71447. (Accessed: 29th August 2018)
19. Albadra, D., Coley, D. & Hart, J. Toward healthy housing for the displaced. *The Journal of Architecture* **23**, 115–136 (2018).
20. McCarthy, P. *Operation Sea Angel: A Case Study*. (US Army, 1994).
21. Hanna, E. G. & Tait, P. W. Limitations to thermoregulation and acclimatization challenge human adaptation to global warming. *International Journal of Environmental Research and Public Health* **12**, 8034–8074 (2015).

22. Camargo, S. J. Global and regional aspects of tropical cyclone activity in the CMIP5 models. *J. Climate* **26**, 9880–9902 (2013).

23. Dwyer, J. G. *et al.* Projected twenty-first-century changes in the length of the tropical cyclone season. *J. Climate* **28**, 6181–6192 (2015).

24. Lewis, S. C. & King, A. D. Evolution of mean, variance and extremes in 21st century temperatures. *Weather and Climate Extremes* **15**, 1–10 (2017).

25. Byrne, M. P. & O'Gorman, P. A. Link between land-ocean warming contrast and surface relative humidities in simulations with coupled climate models. *Geophys. Res. Lett.* **40**, 5223–5227 (2013).

26. Matthews, T. Humid heat and climate change. *Progress in Physical Geography: Earth and Environment* **42**, 391–405 (2018).

27. Haarsma, R. J. *et al.* High Resolution Model Intercomparison Project (HighResMIP v1.0) for CMIP6. *Geoscientific Model Development* **9**, 4185–4208 (2016).

28. Lin, N. & Emanuel, K. Grey swan tropical cyclones. *Nature Climate Change* **6**, 106–111 (2016).

29. Kang, N.-Y. & Elsner, J. B. Trade-off between intensity and frequency of global tropical cyclones. *Nature Climate Change* **5**, 661–664 (2015).

30. Petkova Elisaveta P. *et al.* Towards More Comprehensive Projections of Urban Heat-Related Mortality: Estimates for New York City under Multiple Population, Adaptation, and Climate Scenarios. *Environmental Health Perspectives* **125**, 47–55 (2017).

31. Delworth, T. L., Mahlman, J. D. & Knutson, T. R. Changes in Heat Index Associated with CO2-Induced Global Warming. *Climatic Change* **43**, 369–386 (1999).

32. Diffenbaugh, N. S., Pal, J. S., Giorgi, F. & Gao, X. Heat stress intensification in the Mediterranean climate change hotspot. *Geophys. Res. Lett.* **34**, L11706 (2007).

33. Zhao, Y., Ducharne, A., Sultan, B., Braconnot, P. & Vautard, R. Estimating heat stress from climate-based indicators: present-day biases and future spreads in the CMIP5 global climate model ensemble. *Environ. Res. Lett.* **10**, 084013 (2015).

34. Anderson, G. B., Bell, M. L. & Peng, R. D. Methods to calculate the heat index as an exposure metric in environmental health research. *Environ Health Perspect* **121**, 1111–1119 (2013).

35. Weedon Graham P. *et al.* The WFDEI meteorological forcing data set: WATCH Forcing Data methodology applied to ERA-Interim reanalysis data. *Water Resources Research* **50**, 7505–7514 (2014).

36. Dee, D. P. *et al.* The ERA-Interim reanalysis: configuration and performance of the data assimilation system. *Q.J.R. Meteorol. Soc.* **137**, 553–597 (2011).

37. Rye, C. J., Arnold, N. S., Willis, I. C. & Kohler, J. Modeling the surface mass balance of a high Arctic glacier using the ERA-40 reanalysis. *Journal of Geophysical Research: Earth Surface* **115**, (2010).

38. Kantha, L. Time to replace the Saffir-Simpson hurricane scale? *Eos, Transactions American Geophysical Union* **87**, 3–6 (2006).

39. IBTrACS Science Team. *International Best Track Archive for Climate Stewardship (IBTrACS) Technical Documentation*. (2018).

40. Center for International Earth Science Information Network - CIESIN - Columbia University. Gridded Population of the World, Version 4 (GPWv4): Population Count Adjusted to Match 2015 Revision of UN WPP Country Totals, Revision 10. *Gridded Population of the World (GPW), v4* (2017). Available at: http://sedac.ciesin.columbia.edu/data/set/gpw-v4-population-count-adjusted-to-2015-unwpp-country-totals-rev10/metadata.

41. Morice, C. P., Kennedy, J. J., Rayner, N. A. & Jones, P. D. Quantifying uncertainties in global and regional temperature change using an ensemble of observational estimates: The HadCRUT4 data set. *Journal of Geophysical Research: Atmospheres* **117**,
42. Hansen, J., Ruedy, R., Sato, M. & Lo, K. Global surface temperature change. *Reviews of Geophysics* **48**, (2010).
43. Muller, R. A. *et al.* A new estimate of the average earth surface land temperature spanning 1753 to 2011. *Geoinformatics & Geostatistics: An Overview* **2013**, (2014).
44. Willett, K. M. & Sherwood, S. Exceedance of heat index thresholds for 15 regions under a warming climate using the wet-bulb globe temperature. *Int. J. Climatol.* **32**, 161–177 (2012).
45. Murakami, H. *et al.* Simulation and Prediction of Category 4 and 5 Hurricanes in the High-Resolution GFDL HiFLOR Coupled Climate Model. *J. Climate* **28**, 9058–9079 (2015).
46. Wilks, D. S. *Statistical Methods in the Atmospheric Sciences*. (Academic Press, 2011).
47. Glantz, M. H. The use of analogies: in forecasting ecological and societal responses to global warming. *Environment: Science and Policy for Sustainable Development* **33**, 10–33 (1991).
48. Matthews, T., Mullan, D., Wilby, R. L., Broderick, C. & Murphy, C. Past and future climate change in the context of memorable seasonal extremes. *Climate Risk Management* **11**, 37–52 (2016).

Corresponding Author

Please address all correspondence and requests for the datasets and computer code behind this study to Tom Matthews (t.matthews@lboro.ac.uk).

Author Contributions

TM conceived the study and conducted the analysis. All authors helped design the study and contributed to writing the manuscript.

Competing Interests

The authors declare no competing interests.

Acknowledgements

The authors thank Matthew Foote for discussion about the TC-heat hazard before TCs make landfall.

Figure Captions

Figure 1. Observed TCs and extreme heat. **a**, tracks of the 121 major TCs. Red shows (4) TCs that were followed by HI40.6 within 30 days of landfall. **b**, number of people exposed to a maximum HI of *at least* the value given by the x-coordinate in the 30 days of TC landfall; black shows the number of people (living in the same TC-impacted grid cells) that experience a 99.9th percentile HI (all days of year) of at least the value given by the x-coordinate. Values in brackets in the legend report series' intersection with HI40.6 (grey line).

Figure 2. Seasonal climatologies for major TC occurrence and extent of HI40.6 by ocean basin. **a**, Gaussian smoothed day-of-year climatology for major TC landfall probability (blue) and HI40.6 occurrence (red). All series have been normalized by their respective maximum. Labels above the polar plots denote ocean basin, with the abbreviations defined in the map legend. Note that the angle of rotation indicates day of year (labelled). **b**, map of the domains corresponding to the ocean basins. Red points mark locations impacted by major TCs: only these points in each domain were used to compute the HI40.6 climatology (upper panel).

Figure 3. Composite impact of major TC passage on meteorology across all ocean basins: HI (**a**); 2m air temperature (**b**); specific humidity (**c**); surface air pressure (**d**). The red line highlights zero and the grey shading spans +/- two standard errors of the mean anomaly. Anomalies were calculated from a day-of-year climatology using the same Gaussian kernel procedure as in Fig. 2.

Figure 4. Change in TC-heat hazard under climate change. **a**, expected number of compound TC-heat events as function of global warming amount. Shading spans the uncertainty range from repeating the analysis using the 5th and 95th percentiles of pattern-scaling coefficients; black line uses the ensemble mean coefficients; red dot is the observed TC-heat event rate. **b**, as upper but for the expected number of people directly impacted by TC-heat events. **c**, same as middle/upper, but for mean maximum HI post TC landfall (see Methods). The red dotted line (slope annotated) is the best-fit linear approximation of the black curve.

Figure 5. Analogue major TCs under climate warming. Major *probable* TC tracks (with at least a 50% chance of experiencing HI40.6 in the 30-days following landfall) are plotted for the different amounts of global warming (**b**-**d**; shown above each map). For the (1981-2010) baseline (**a**), we also indicate (with dotted blue lines) those *possible* TC tracks (with non-zero probability of being followed by HI40.6). On each panel, the expected number of compound TC-heat hazards in a 30-year period E[N] is provided (rounded to the nearest integer).

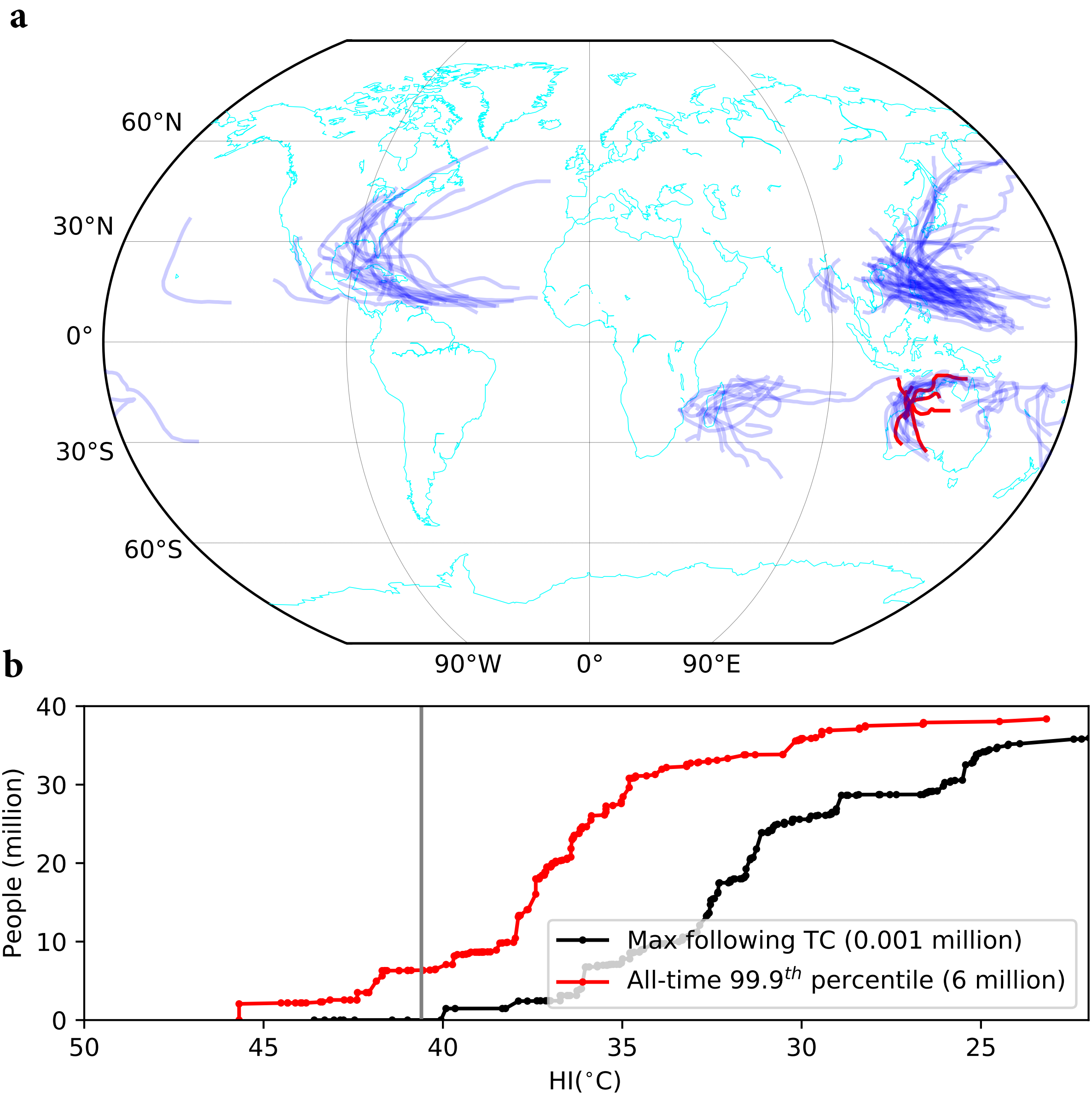
a
60°N
30°N
0°
30°S
60°S
90°W
0°
90°E
b
People (million)
HI(°C)
Max following TC (0.001 million)
All-time 99.9th percentile (6 million)

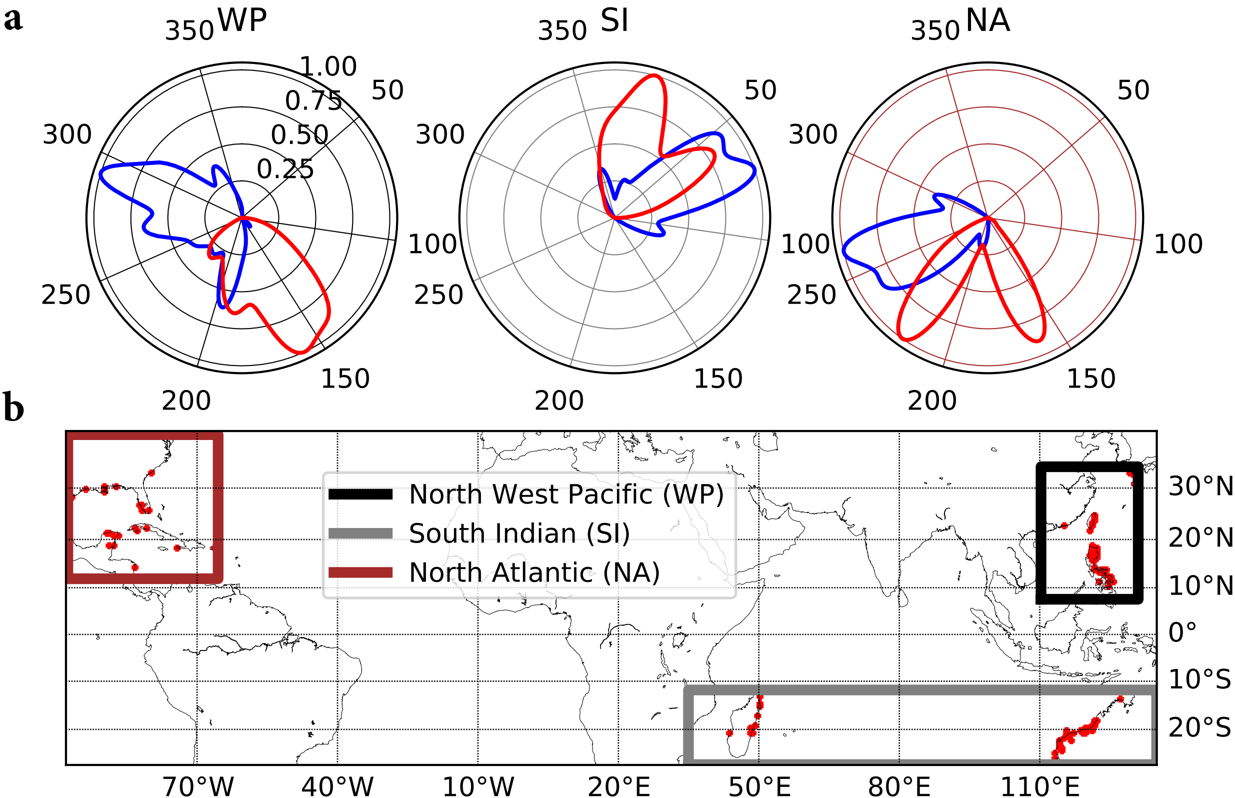
a
WP
SI
NA
350
50
100
150
200
250
300
1.00
0.75
0.50
0.25
b
North West Pacific (WP)
South Indian (SI)
North Atlantic (NA)
30°N
20°N
10°N
0°
10°S
20°S
70°W
40°W
10°W
20°E
50°E
80°E
110°E

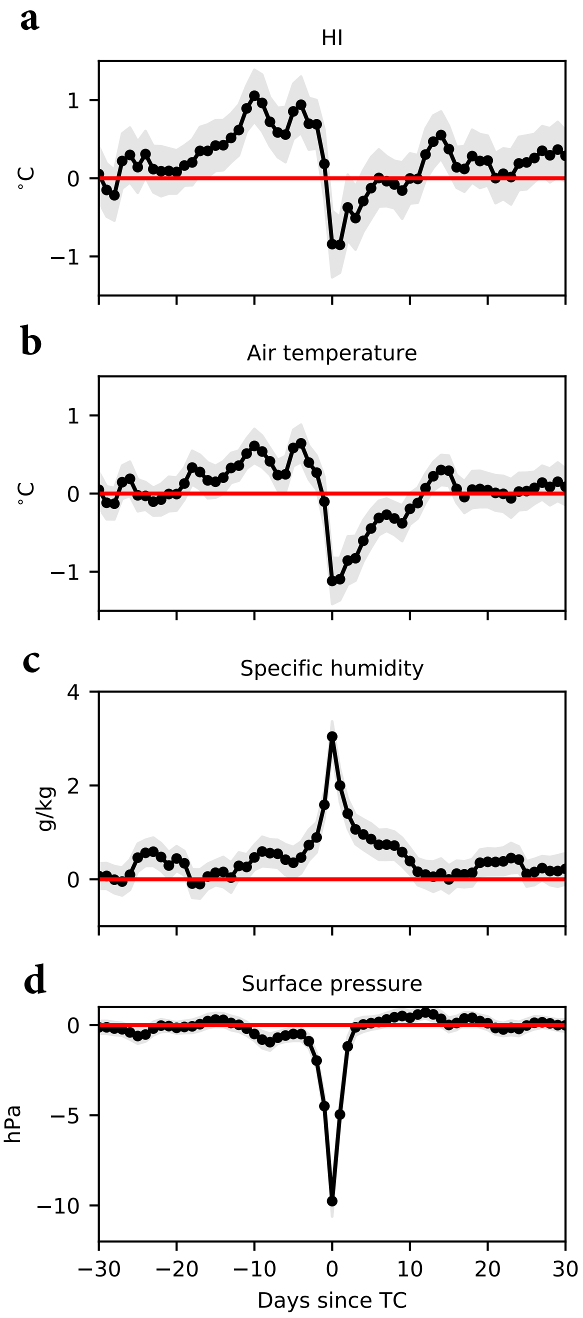

a
HI
°C
1
0
−1
b
Air temperature
°C
1
0
−1
c
Specific humidity
g/kg
4
2
0
d
Surface pressure
hPa
0
−5
−10
−30
−20
−10
0
10
20
30
Days since TC

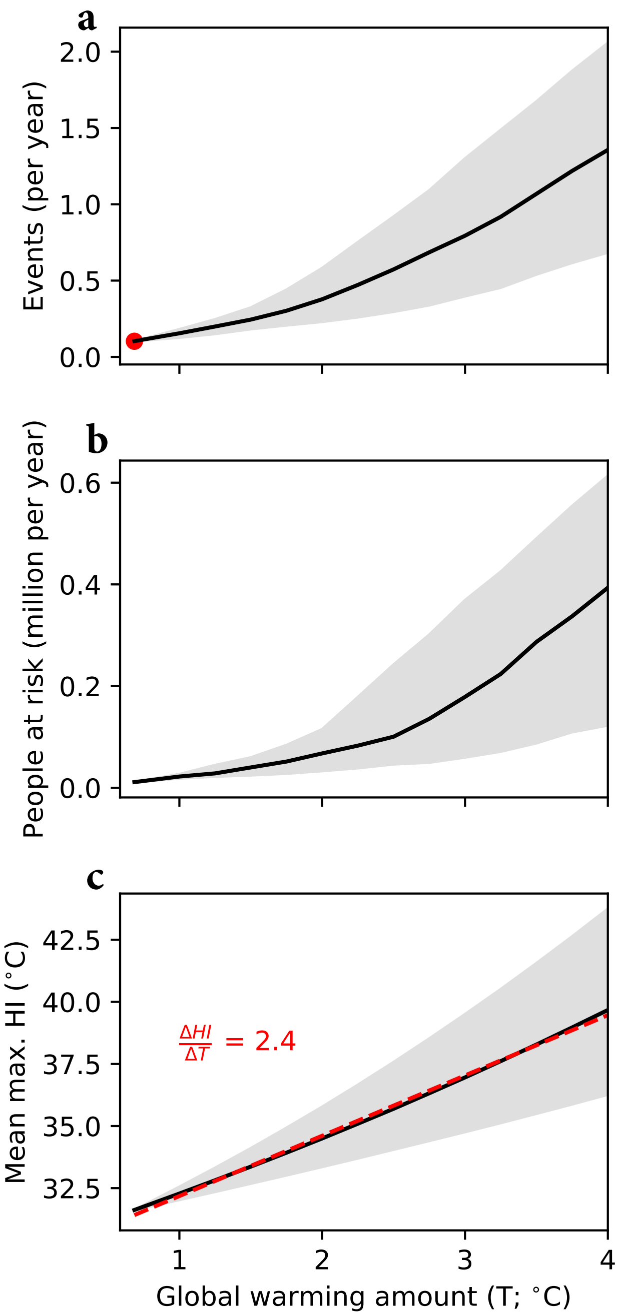
a
Events (per year)
0.0
0.5
1.0
1.5
2.0
b
People at risk (million per year)
0.0
0.2
0.4
0.6
c
Mean max. HI (°C)
32.5
35.0
37.5
40.0
42.5
$\frac{\Delta HI}{\Delta T}$ = 2.4
1
2
3
4
Global warming amount (T; °C)

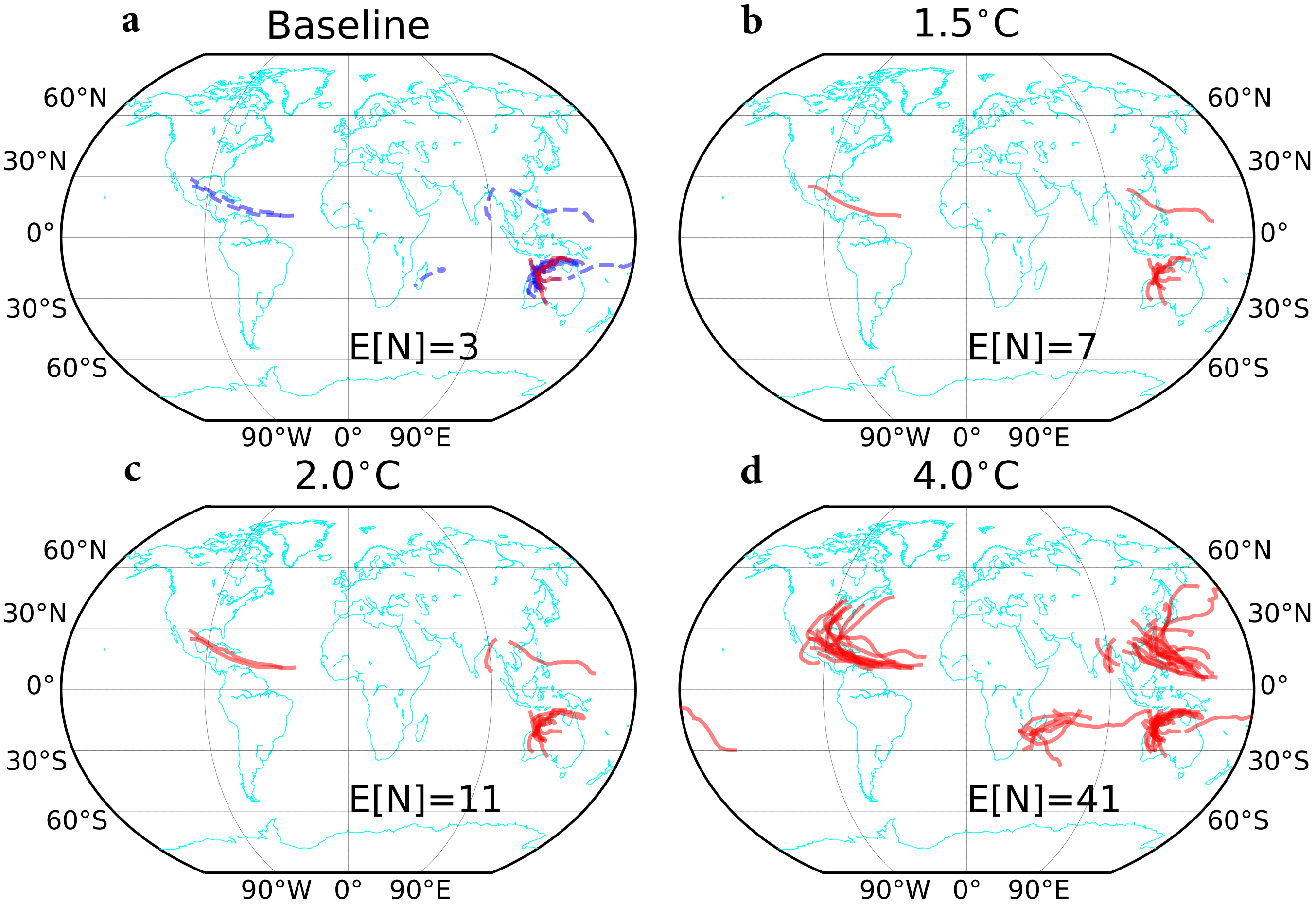
a
Baseline
b
1.5°C
c
2.0°C
d
4.0°C
60°N
30°N
0°
30°S
60°S
90°W
0°
90°E
E[N]=3
E[N]=7
E[N]=11
E[N]=41